THE ASTRONOMICAL JOURNAL VOLUME 113, NUMBER 5 MAY 1997

BVRI AND Hα SURFACE PHOTOMETRY OF THE TRIPLE-RINGED GALAXY IC 4214

M. F. SARAIVA[1]

Departamento de Astronomia, Instituto de Física, Universidade Federal do Rio Grande do Sul, Av. Bento Gonçalves, 9500 - C.P. 15051, 91501-970, Porto Alegre, RS, Brazil

Received 1996 November 1; revised 1997 February 6

ABSTRACT

BVRI and Hα CCD surface photometry is presented for the Sab system IC 4214, an example of a galaxy with three rings and no conventional bar. We obtained isophote maps, luminosity profiles, and basic photometric parameters. The photometry suggests the galaxy has three major structural components: the nuclear bulge, the disk, and a non-axisymmetric component that is a mixture of bar, inner ring and lens. The bar is a very weak feature that appears clearly only in the *I* band. Even so, the non-axisymmetric component contributes 23% to the total *I* luminosity. The Hα emission is concentrated mostly in the nuclear ring and in the two spiral arms that form the inner ring. Both the inner ring and nuclear ring are blue compared with their surroundings, and must contain regions of star formation mixed with dust. The existence of rings in non-barred and weakly barred galaxies is still not well explained by theories of ring formation. This galaxy seems to be a case like others that have appeared in the literature, where the bar was stronger in the past, and now is dissolving. © *1997 American Astronomical Society.* [S0004-6256(97)03105-1]

1. INTRODUCTION

Rings are very common galactic features that appear in about 50% of disk galaxies (Buta 1986b), preferentially in the barred ones. A quantification of this preference is given by the sample of ringed galaxies of the Catalog of Southern Ringed Galaxies (CSRG—Buta 1995), where 50% of the galaxies are barred, 27% are weakly barred, and only 23% have no bar at all. The observation of this apparent connection between rings and bars is as old as the observation of rings themselves, and early motivated the search for an explanation of the rings formation in terms of the bar potential. Today it is largely accepted that rings form by gas accumulation at resonances, under the influence of gravitational torques exerted by the bar potential on the gas (Combes 1996). Nevertheless, this theory cannot explain satisfactorily the existence of rings in unbarred or weakly barred galaxies.

The properties of rings in four weakly-barred galaxies were studied by Buta, in a series of papers (Buta 1990a, 1990b, 1990c, 1990d), in which he founded that the rings in these galaxies, although being mostly stellar in nature, show some similarities with the rings in more conventionally barred galaxies. Buta concluded that, unless the presence of a bar is not necessary for the formation of stellar rings, these galaxies must have had stronger bars in the past, and are now going through a process of bar dissolution.

A similar scenario, with total destruction of the bar, has been recently proposed by Athanassoula (1996) to explain the rings in the SA galaxy NGC 7217. Nevertheless, Palouš & Jungwiert (1996), based on *N*-body simulations, claim that even very weak bars or triaxial distortions are able to generate long-lasting gaseous rings.

Since the number of galaxies of this kind studied so far is still very small, it seems interesting to examine the case of IC 4214: a large, moderately bright example of a galaxy with no conventional bar and with the three main ring types possible in a galaxy: a nuclear ring, an inner ring, and an outer ring. In the CSRG it is classified as $(R_1')SAB(r)a$. It shows close similarities with the Seyfert S0/a galaxy NGC 3081 (Buta 1990a).

The three rings of IC 4214 were previously shown in the $(B-I)$ map by Buta & Crocker (1991), and their diameters (1.97×1.21 arcmin, 0.91×0.48 arcmin, and 0.146×0.141 arcmin) were measured by Buta & Crocker (1993). The orientation of the inner and outer ring with respect to the bar are given in the CSRG as 6.5 degrees and 34.4 degrees, respectively.

Multi-aperture *UBVRI* photoelectric photometry was obtained by Buta and Crocker (1992, hereafter BC92), from which they derived integrated magnitudes and colors. Integrated photometric parameters in the *I*-band were also measured by Han (1992), through surface photometry.

Maia *et al.* (1987) identified IC 4214 as a LINER on the basis of its optical spectrum, but its *IRAS* flux densities were identified as normal by Rush *et al.* (1993).

The heliocentric velocity of IC 4214 in the RC3 is 2281 km s^{-1}. Correcting for a dipole Virgo-centric flow following Tammann & Sandage (1985), it becomes 2488 km s^{-1}. Using a Hubble constant of 80 km s^{-1} Mpc^{-1}, then the distance is nearly 31 Mpc, and the scale factor is 1 arcsec =151 pc. Table 1 lists some catalogue parameters of IC 4214.

In this paper we present *BVRI* and Hα CCD photometry for IC 4214, to provide more information on its basic properties and structure. The observations are described in Sec. 2. Sections 3 and 4 discuss the morphology of the galaxy as seen in the broad band images and in the emission line im-

[1]Visiting Astronomer, Cerro Tololo Inter-American Observatory. CTIO is operated by AURA, Inc. under contract to the National Science Foundation.

 0004-6256/97/113(5)/1607/11/$10.00

TABLE 1. RC3 parameters for IC 4214.

Right Ascension (1950)	13h 17.7min
Declination (1950)	−32°06′
ℓ, b	309.39, 30.44
Morphological type	$(R')SB(r)ab$
Isophotal diameter D_{25}	2.24′
Face-on isophotal diameter D_0	2.34′
Disk axis ratio R_{25}	1.73
Position angle of the major axis	176°
Heliocêntric radial velocity	2281 km s^{-1}
Total magnitude B_T	12.27
Corrected total magnitude B_T°	11.65
Integrated color $(B-V)_T$	0.85
Corrected integrated color $(B-V)_T^\circ$	0.71
Internal absorption	0.30

age; in Sec. 5 we present the analysis of the data, and in Sec. 6 we summarize the results.

2. OBSERVATIONS

The observations were made in 1992 June using the TEK 1024 CCD at the 91 cm telescope of the Cerro Tololo Inter-American Observatory (CTIO). The CCD was binned 2×2 so the final scale of the image was 0.792 arcsec/pixel. The filters used were B, V, R, and I, and two narrow filters of 75 Å wide centered at 6649 Å (to isolate the Hα+[N II] emission line at the redshift of the galaxy) and at 6477 Å (to isolate a nearby region of stellar continuum). The quarter moon was 52 degrees north from the galaxy during the observations. A log of the observations is given in Table 2.

The images were corrected for bias and flat-field using standard IRAF routines, and the multiple exposures in each filter were combined. The sky background of the final *BVRI* images was determined using the Numerical Mapping Technique (Jones *et al.* 1967) adapted for CCD images by S. Odewahn (Nummapi code). We used a 2D 4th degree polynomial of fourteen terms to map the four borders of the frames, each border 70 arcsec wide, after cleaning all the stars in the borders using appropriate IRAF routines. 4th degree was chosen because the sky was not flat, and 4 was the highest permissible degree for both x and y compatible with the size of the sky field compared with the galaxy field, according to the criterion to prevent instability discussed by Jones *et al.* (1967). The sky map thus obtained was interpolated under the galaxy.

The photometric calibration of the *BVRI* data to the Johnson-Cousins system was made using observations of 10 standard stars in the E-Regions (Graham 1982), to determine

TABLE 2. Observations.

Filter	Exposure time (sec)	Telescope	FWHM (″)
B	3×200	91 cm - CTIO	2.2
V	2×120	91 cm - CTIO	2.1
R	2×60	91 cm - CTIO	1.9
I	1×60	91 cm - CTIO	2.1
H_{6649}	5×600	91 cm - CTIO	2.0
H_{6477}	3×600	91 cm - CTIO	2.0

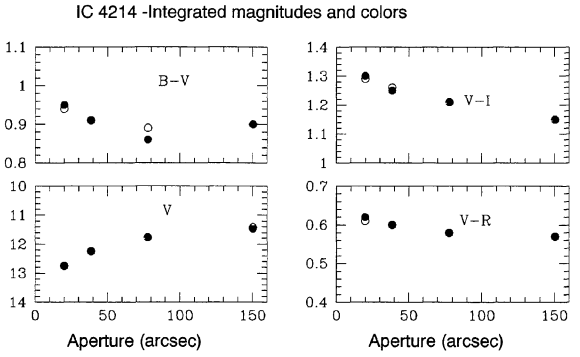

FIG. 1. Comparison between our CCD photometry (solid dots) and the photoelectric photometry by BC92 (circles).

the color terms, and then adjusting the zero points to fit the photoelectric photometry of BC92. The mean differences between zero points from the stars only and zero points adjusted to photoelectric photometry were: $\langle B-V\rangle_{PP}-\langle B-V\rangle_{SS}=-0.002\pm0.018$, $\langle V\rangle_{PP}-\langle V\rangle_{SS}=0.015\pm0.007$, $\langle V-R\rangle_{PP}-\langle V-R\rangle_{SS}=0.008\pm0.007$, and $\langle V-I\rangle_{PP}-\langle V-I\rangle_{SS}=0.072\pm0.018$.

The final transformations equations were:

$$B-V=1.29(b-v)_o-0.534,$$

$$V=v_o-0.025(B-V)+22.59,$$

$$V-R=0.969(v-r)_o-0.081,$$

$$V-I=(v-i)_o+0.604.$$

Figure 1 shows the comparison between our CCD photometry and the photoelectric photometry. The agreement is within 0.02 mag, and no systematic deviation is observed. This give us confidence that the sky subtraction is correct, despite the sky not being flat.

To obtain the final continuum subtracted Hα emission line image we proceeded in two different ways: first, we scaled the continuum image to match the intensities of the emission image using the intensities of the stars in the two images, and then made the subtraction; second, we scaled the two images using the parameters obtained from a linear regression of the mean intensity of the isophotes in both images. Both techniques gave the same result. We made no calibration, and no correction for spectral color, since the difference between the central wavelength of the continuum filter and the emission filter is small enough that no significant spectral color terms are expected.

3. MORPHOLOGY

The global morphology of IC 4214 is illustrated in the images in Figs. 2 and 3. The main body of the galaxy is bounded by an oval structure that might be identified as a lens (Fig. 2). The lens has at its ends two faint and slightly curved regions that seem to be two spiral arms that connect it to the outer ring. The conjunction lens+spirals composes a larger and pointed oval resembling a fat S-shaped figure, that fills diagonally the outer ring. Figure 3 displays the structure inside the lens, that here appears as a mixture of lens and

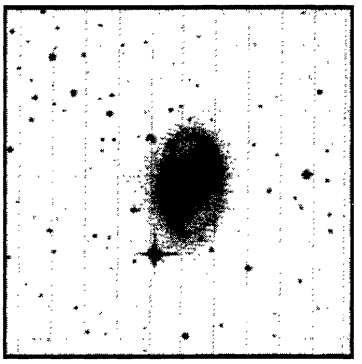

FIG. 2. Reproduction of the digitalized SRC plate, showing the external parts of IC 4214. The displayed field of view is 6.6′×6.6′, the same size as the entire CCD frames. North is up, east is to the left.

inner pseudo-ring. The inner ring is composed of two spiral arms, the northern one more closed and patchy, the southern one more open and very bright until its southeast point, where it seems to end. In reality it becomes very faint from this point on, but continues until past the point where the northern arm begins. In the inner side of the northern arm appears a dust lane, that departs from the bulge and is quite straight until its ends, where it curves following the spiral arm. The southern arm also seems to have a very diffuse spiral-shaped dust lane. Curved dust lanes are common in the leading side of weak bars (Athanassoula 1992). The bar is not clear in this image; it could be classified as a mixture of the types "ring/lens" bar-like distortion and "spiral" distortion (Buta 1986a). The nuclear bulge is very elongated and slightly squarish in the north side. The isophotes inside it are slightly elongated to the east, suggesting the existence of a small nuclear bar oriented almost perpendicularly to the direction of the inner ring.

Comparing Figs. 2 and 3 we can notice a repetitive pattern in this morphology, the structure inside the inner ring mimicking the global structure of the galaxy.

The $B-I$ color index map (Fig. 4) shows the nuclear and inner ring, that appear as blue enhancements compared with their surroundings. The nuclear ring is much bluer and wider in the northeast side, showing a crescent shape. In the southern side it is split by a dust lane, which emerge southern of the nucleus and wraps westward around the nuclear ring until the north. The part of the nuclear ring split by the dust lane seems to have been displaced southward, giving rise to the isolated blue concentration located 10″ southern of the nucleus. The inner ring is very elongated, and is well defined along the north-east-south arc. In the west side it is wider and fainter, because in this side the southern arm surpass the northern one without touching it, so the ring is not closed.

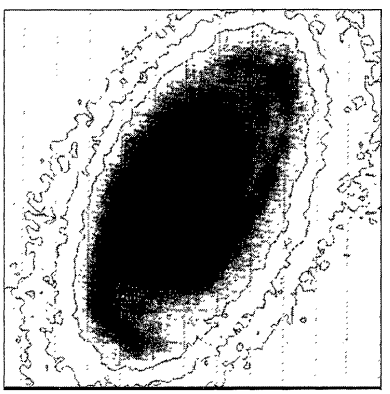

FIG. 3. Combination of the B, V, R, and I CCD images of IC 4214, showing the parts of the galaxy internal to the primary lens. The field is 70″×70″.

FIG. 4. $B-I$ color map of the inner region of IC 4214, showing the inner and nuclear rings of IC 4214 as blue features. The field of view is 64″×64″. North is up, east is to the left.

Looking at this $B-V$ map, we can see the dust lines in the inner part of the inner ring in the west side, but not in the east side. This does not mean necessarily that there are no dust lanes in the east side: it is possible that they exist and are hidden by the ring itself. If this is true, then in the west side the inner part of the inner ring is turned toward us, and in the east side the outer part of the inner ring is turned toward us. Consequently this would mean that the east side is the near one.

4. DISTRIBUTION OF THE IONIZED GAS

The Hα map (Figs. 5 and 6) shows the locations of the emission regions of the galaxy, that are mostly concentrated within the nuclear region. The nuclear emission is ring-like, with a stellar-like concentration at the very center. The ring is composed of isolated knotty regions that fit well in the "ring nuclear emission region" class of Pogge (1989). The two strongest emission regions are located symmetrically in both sides of the nucleus, forming a "three blob" nuclear bar. The major axis of this "bar" does not coincide with the major axis of the nuclear bar seen in Fig. 3 though, being displaced 10° respected to it.

In the inner ring region the gas is distributed along the two spiral arms that form the inner ring. The emission along the southern arm is stronger than along the northern one. There is no special concentration of gas at the major axis of the inner ring, as is in general observed in ringed galaxies (Crocker *et al.* 1996; Wosniak *et al.* 1995). There is no clear emission along the bar.

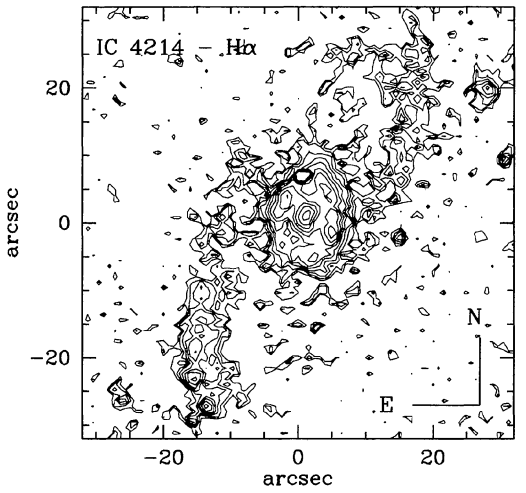

FIG. 5. Hα continuum subtracted isophote map of the inner region of IC 4214. The isophotal levels are arbitrary. Only the regions where the emission is significant are shown. The two bright, star-like regions at the ends of the southern arm, do not seem to be emission regions, but bad subtracted stars. The field of view is 64″×64″.

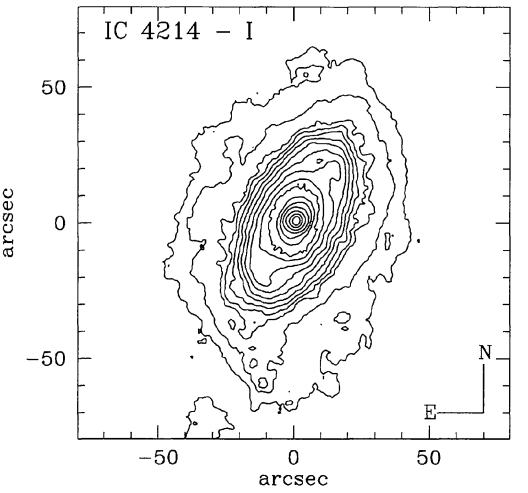

FIG. 7. *I*-band isophote map of IC 4214. The two outer isophotes are μ_I=21.5 and 22.0 mag s^{-2}, using a 7.9″×7.9″ box average. The next 8 isophotes range from μ_I=21.0 to 19.25 mag s^{-2}, in steps of −0.25 mag s^{-2}, and were smoothed using a 3.9″×3.9″ box average. The seven inner isophotes range from μ_I=19 to 16 mag s^{-2}, in steps of −0.5 mag s^{-2}, and were not smoothed.

5. ANALYSIS OF THE DATA

5.1 Isophotes and Geometric Parameters

An isophote map in the *I* band is shown in Fig. 7, where it appears quite clear that the galaxy has a bar nearly aligned with the pseudo inner ring. This bar is almost invisible in *B*. Galaxies that appear unbarred at visual wavelengths and show a bar when observed at infrared are becoming increasingly frequent in literature [e.g., NGC 1566 (Hackwell & Schweizer 1983), NGC 1068 (Thronson *et al.* 1989), and NGC 253 (Forbes & DePoy 1992)]. According to these authors, the bars in these galaxies are hidden by the dust, or are made up of older, redder stars. IC 4214 has a high inclination and dust absorption may be important, but the kind of stellar population may also be contributing for hiding the bar. Figure 8 shows an isophote map in the *I* band for the nuclear region. Here the flattening of the western side of the "nuclear bar" isophotes is not as strong as it appears in Fig. 3, but still exists. If the nuclear bar is real, it is possible that it is not in the same plane of the primary bar, and its western side is behind the primary bar.

In Table 3 we give the dimensions of the several substructures identified in the galaxy. At the level of detection we have, the bar has practically the same size and axis ratio as the inner ring. The nuclear bar is a little more elongated than the nuclear ring. The sizes of the three rings are quite similar to those measured by Buta and Crocker (Sec. 1).

According to Athanassoula *et al.* (1982), and Buta (1986, 1990a), the size ratios between the rings can be used to iden-

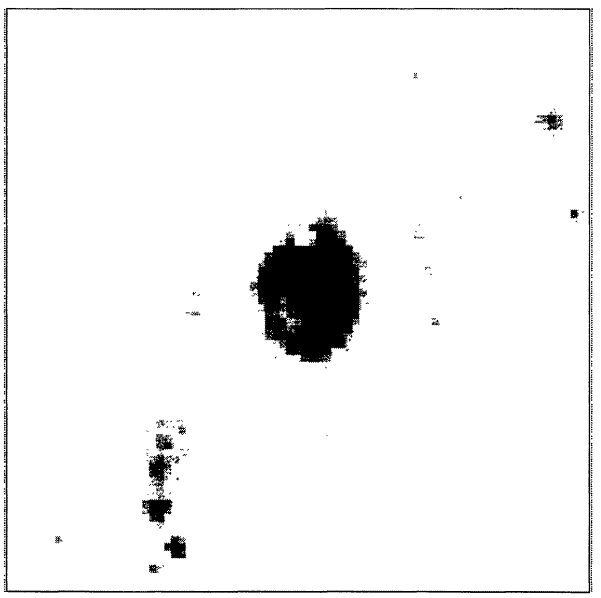

FIG. 6. Hα continuum subtracted map showing the nuclear emission of IC 4214. The field of view is 64″×64″.

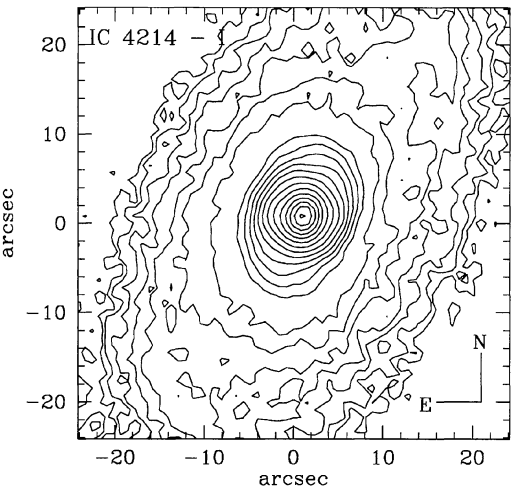

FIG. 8. *I*-band isophote map of the inner region of IC 4214. The isophote levels range from μ_I=15.5 to 20.5 mag s^{-2}, in steps of −0.25 mag s^{-2}.

TABLE 3. Dimensions of structures of IC 4214.

Feature	Apparent diameter[a]	Axis ratio (b/a)
outer ring	120 arcsec, 18 kpc	0.65
pointed oval	100 arcsec, 15 kpc	0.50
primary lens	64 arcsec, 9.6 kpc	0.50
inner ring	54 arcsec, 8.4 kpc	0.48
bar	51 arcsec, 7.7 kpc	0.46
nuclear bulge	24 arcsec, 3.6 kpc	0.65
nuclear ring	9 arcsec, 1.3 kpc	0.95
nuclear bar	8 arcsec, 1.2 kpc	0.87

[a]The rings were measured at the peak of brightness, the other structures at the outer edges.

tify them with the locations of the principal resonances. For IC 4214 the projected ratios are $D(R)/D(r)=2.2$, $D(R)/D(nr)=13.3$, and $D(r)/D(nr)=6$, which are in good agreement with the mean size ratios of rings measured for strong barred galaxies (Buta & Crocker 1993).

Following Buta (1990a), we used the ratio between the outer ring and the face-on geometric mean inner ring ($D(R)/\langle D(r_o)\rangle=2.7$) to compare with theoretical values, instead of the projected ratio. The predicted value for a constant-velocity rotation curve is $r(OLR)/r(UHR)=2.6$ (Athanassoula *et al.* 1982). Then the observed ratio supports the interpretation of the inner ring and the outer ring are linked to the resonances OLR and ILR, respectively.

The projected outer-to-nuclear ring ratio is large compared with the ratio $r(OLR)/r(ILR)=5.8$ (Athanassoula *et al.* 1982) expected for a constant rotation curve. But Buta (1990a) already pointed that this ratio is not very useful for resonance identifications.

Ellipse fits to the B, V, R, and I isophotes were made using the task *ellipse* in the STSDAS package, to determine the position angle (θ) of the isophotes, ellipticity (ϵ), and the Fourier amplitudes of deviations from perfect ellipticity ($\cos 4\theta$ term, $B4$). Figure 9 shows the variation of these three parameters with the ellipse semi-major axis a. The locations of the nuclear ring ($a=4.5''$, $\theta=-44°\pm4.5°$, $\epsilon=0.05\pm0.01$), inner ring ($a=27''$, $\theta=-30°\pm1.4°$, $\epsilon=0.53\pm0.02$), and outer ring ($a=60''$, $\theta=-14°\pm9°$, $\epsilon=0.35\pm0.09$) are marked. The nuclear ring is the roundest one, and the inner ring is the more elongated one, as is normal for rings in other double-ringed or triple-ringed galaxies.

The ellipticity and position angle of the isophotes have nearly the same behavior in V, R, and I. In B they behave a little differently, mainly in the region between 10″ and 15″, where possibly the presence of dust is disturbing the B isophotes. In the range from 0″ to 35″ the graph of ellipticity resembles the "barred + twisted isophotes" case in Wosniak *et al.* (1995), with the first maximum at the borders of the nuclear bulge and the real maximum at the position of the inner ring. The position angle varies strongly in the nuclear region. The behavior of both ellipticity and position angle of the inner isophotes is consistent with the galaxy having a triaxial bulge and/or a nuclear bar (Shaw *et al.* 1995, Wosniak *et al.* 1995). In the region between 35″ and 50″ (pointed oval region), the ellipticity remains almost constant, then drops quickly in the outer ring and stabilizes again for the external isophotes ($a>65''$). Assuming the axial ratio

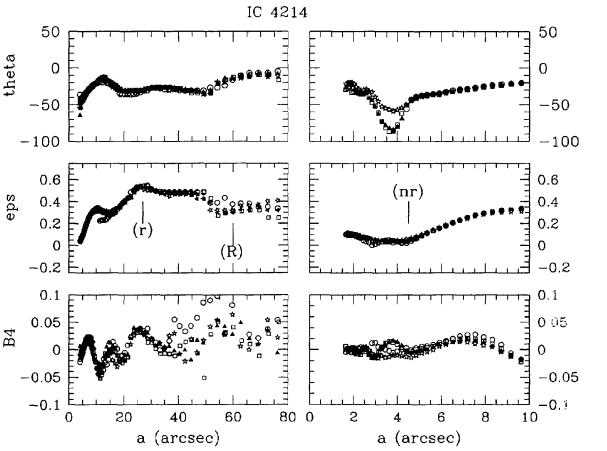

FIG. 9. Isophotal parameters of IC 4214 as a function of the ellipse semi-major axis. The symbols circles, squares, triangles, and stars represent the filters B, V, R, and I, respectively. The right plots are the same as the left ones, but show only the expanded innermost region.

($=1-\epsilon$) of these external isophotes corresponds to the apparent axial ratio of the disk, and assuming the intrinsic axial ratio of the disk is 0.226 (following Bottinelli *et al.* 1983, for *Sa*'s), then the inclination of the disk is 51°. The position angle of the disk, measured at the same isophote, is 172°.

The term B4 has a complicated behavior; the more significant deviations from elliptical shape indicate pointed isophotes at $a=7''$, boxy isophotes at $a=11''$ (borders of nuclear bulge), and pointed isophotes at $a=27''$ (inner ring). The outer isophotes become very pointed again, with a peak at $a=50''$, in the position where the spiral arms that connect to the outer ring.

5.2 Integrated Photometric Parameters

The B, V, R, and I magnitudes and colors, obtained by integrating the light in elliptical annuli with the shape of the outer isophotes ($b/a=0.65$, P.A.$=172°$), are listed in Table 4. The isophotes are quoted by their semi-major axis a and by their equivalent radii, defined by $r^*=\sqrt{A/\pi}$, where A is the area enclosed by the elliptical aperture.

For obtaining the total magnitude B_T, we calculated an elliptically averaged profile, and extrapolated it to infinity by assuming an exponential distribution after $a=100''$. The amount of extrapolation required was 7%, and the resulting total magnitude was $B_T=12.27\pm0.04$. Correcting for galactic extinction, internal absorption, and red-shift, following RC3, this leads to the corrected total magnitude $B_T^\circ=11.66$. For a distance of 31 Mpc, this corresponds to an absolute magnitude of $M_T^\circ(B)=-20.81$. The main photometric parameters of the galaxy are collected in Table 5. The total colors were quoted assuming the integrated colors do not change significantly after the last aperture in Table 4. The colors were corrected for galactic extinction, internal absorption, and red-shift, using the color excesses and k-corrections deduced by BC92. The corrected color $(B-V)_T^\circ=0.74$ is typical of Sa galaxies (de Vaucouleurs 1977).

TABLE 4. Integrated magnitudes and colors for IC 4214.

r^*	a	B	V	R	I	$B-V$	$V-R$	$V-I$
0.01	0.0	27.158	26.070	25.298	24.692	1.088	0.772	1.378
4.04	5.0	14.567	13.585	12.966	12.275	0.982	0.619	1.310
8.07	10.0	13.862	12.918	12.320	11.643	0.944	0.598	1.275
12.10	15.0	13.559	12.617	12.025	11.354	0.942	0.592	1.263
16.13	20.0	13.329	12.394	11.809	11.147	0.935	0.585	1.247
20.16	25.0	13.148	12.217	11.639	10.987	0.931	0.578	1.23
24.19	30.0	12.997	12.075	11.502	10.859	0.922	0.573	1.216
28.23	35.0	12.883	11.964	11.395	10.762	0.919	0.569	1.202
32.26	40.0	12.800	11.884	11.317	10.692	0.916	0.567	1.192
36.29	45.0	12.734	11.819	11.255	10.635	0.915	0.564	1.184
40.32	50.0	12.672	11.760	11.198	10.585	0.912	0.562	1.175
44.35	55.0	12.615	11.704	11.147	10.541	0.911	0.557	1.163
48.38	60.0	12.562	11.653	11.100	10.499	0.909	0.553	1.154
52.41	65.0	12.515	11.608	11.057	10.462	0.907	0.551	1.146
56.44	70.0	12.479	11.573	11.024	10.434	0.906	0.549	1.139
60.48	75.0	12.449	11.545	10.998	10.412	0.904	0.547	1.133
64.51	80.0	12.424	11.523	10.975	10.396	0.901	0.548	1.127
68.54	85.0	12.400	11.506	10.956	10.381	0.894	0.550	1.125
72.57	90.0	12.379	11.491	10.940	10.369	0.888	0.551	1.122
76.60	95.0	12.362	11.482	10.928	10.360	0.880	0.554	1.122
80.63	100.0	12.351	11.475	10.918	10.356	0.886	0.557	1.119

5.3 Luminosity and Color Profiles

The luminosity and color profiles obtained from the ellipse fitting of the isophotes are shown in Fig. 10. The errors in the magnitudes were obtained from the rms scatter of the intensity along the fitted ellipse. The errors in the colors were calculated by summing the squares of the errors in the surface brightness. The most prominent feature in the profiles is the hump between 20″ and 35″, corresponding to the inner ring region. The contrast of the hump is about the same in the four passbands, but in B it appears larger because the bulge profile decreases more quickly from I to B, either because of the stronger interaction of the bar with the bulge in I, or because of the larger effect of the absorption in B, or both. The $B-V$ profile presents a red bump in the region between the nuclear ring (narrow dip at 5″) and the inner ring (shallow dip from 20″ to 35″), that does not appear in $V-R$ and $V-I$.

Figure 11 displays the profiles along the main axis of the inner ring. The error bars in magnitude represent the errors due to readout noise and uncertainty in sky subtraction. The errors in the color indices were calculated by adding quadratically the errors in surface brightness. The positions of the nuclear ring (nr), inner ring (r), and outer ring (R), are marked. Due to the different orientation of the outer ring with respect to the inner ring, the outer ring is intercepted

TABLE 5. Photometric parameters of IC 4214.

Distance (H=80 km s^{-1} Mpc^{-1})	31 Mpc
Disk axial ratio	b/a=0.65
Inclination	51°
Disk position angle	172°
Total apparent magnitude (B)	B_T=12.27±0.04
Effective equivalent radius (B)	r_e=22″±2″
Equivalent B magnitude	B_e=13.02
Corrected total apparent magnitude	B_T°=11.66
Corrected total absolute magnitude	$M_T^\circ(B)$=−20.81
Total apparent colors	$(B-V)_T$=0.88
	$(V-R)_T$=0.56
	$(V-I)_T$=1.12
Total corrected colors	$(B-V)_T^\circ$=0.74
	$(V-R)^\circ$=0.50
	$(V-I)^\circ$=0.97
Effective colors (at r_e=22″)	$(B-V)_e$=0.93
	$(V-R)_e$=0.58
	$(V-I)_e$=1.22
Effective average surface brightness (B)	$\mu_e(B)$=20.85
Total luminosity ($M_\odot$ (B)=5.48)	$L_T(L_\odot)$=3.2×10^{10}

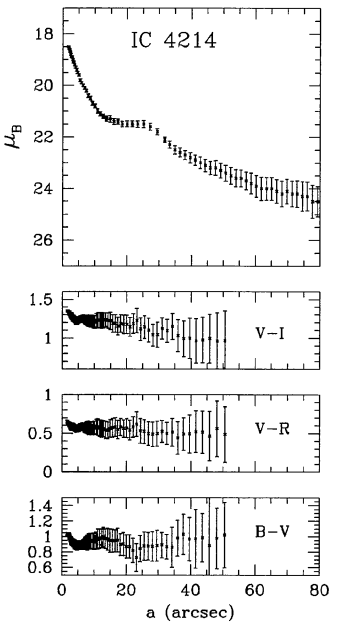

FIG. 10. Surface brightness and color profiles averaged over isophotes, as a function of the semi-major axis of the ellipse fitted to the isophote.

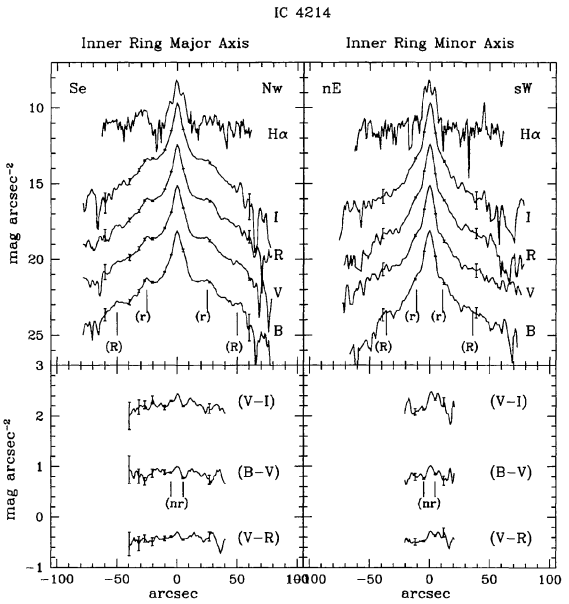

FIG. 11. Luminosity and color profiles along the major and minor axis of the inner ring. The V, R, I, $V-R$, and $V-I$ are offset by -2, -4, -6, -1 and $+1$, respectively. The point zero of the Hα profile is arbitrary. The positions of the outer ring (R), inner ring (r),and nuclear ring (nr), are marked.

along directions that are intermediate between its major and minor axis, so it appears shorter and rounder than it is in the image.

The nuclear ring is very remarkable in the Hα profiles (two narrow bumps next to the nucleus). In the *BVRI* profiles it causes the slightly convex shape of the profiles in the bulge region. In the inner ring region, the profiles are nearly uniform along the major axis (shoulder shaped), and decrease very quickly along the minor axis. The southeast shoulder has a strong hump next to its end, that is increasingly pronounced from I to B, corresponding to the position where the profile cuts the brighter part of the inner ring. These kinds of uniform profiles, identified as "flat bars" profiles by Elmegreen & Elmegreen (1985), are characteristic of strong barred galaxies. In IC 4214 this kind of profile more possibly is being caused by all the bar/inner ring/lens zone than by the weak bar alone. According to Kormendy (1982), lenses and bars have similar major axis brightness profiles (nearly constant interior to a sharp outer edge), their difference is in the minor axis, thus it is difficult to differentiate these two features in inclined galaxies. The high inclination itself may somehow propitiate the observation of these "flat bars" profiles, since other highly inclined galaxies present this feature in their profiles, barred or not, e.g. NGC 3115 (Tsikoudi 1979), NGC 4111 and NGC 4672 (Burstein 1979), NGC 6835 (Schröder *et al.* 1990).

The color profiles have a low signal-to-noise ratio, the only variations that are significant compared with the error bars are the ones within the bulge region. The nuclear ring makes a wide blue dip in the NW side of the major axis profile, but this dip does not have symmetrical counterpart in the opposite side of the profile. In the minor axis the nuclear ring is almost imperceptible, and merges with the inner ring in the NE side. Compared with the nuclear ring of NGC

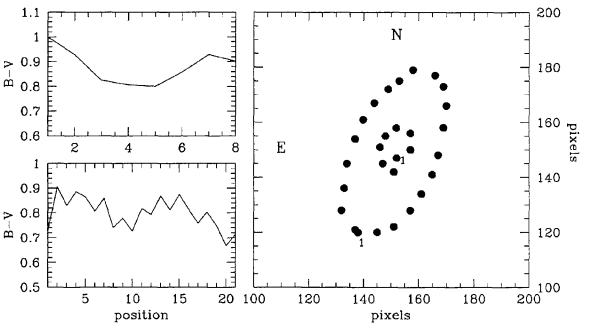

FIG. 12. $B-V$ colors along the inner (bottom) and nuclear (top) rings as a function of the position angle (north to east). The position of the apertures used are shown in the right panel. To facilitate the identification of the corresponding points in the right and left panels we marked the first point measured in each ring with the number 1.

4314 (Benedict *et al.* 1992), this nuclear ring seems much less prominent and is 0.1 mag redder in $B-V$.

5.4 Ring Colors

We measured the colors along the inner and nuclear rings by integrating the surface photometry within small circular apertures roughly equally spaced. The $B-V$ colors are plotted in Fig. 12. The behavior of the inner ring colors is near-sinusoidal with total amplitude of 0.2 mag in $B-V$. The bluest points are in the regions immediately leading the major axis of the inner ring (supposing the arms are trailing), and the reddest points are located in the regions between the major and minor axis, in the side trailing the major axis.

The average observed colors of the inner ring, are $B-V=0.82$, $V-R=0.52$, and $V-I=1.11$, that do not imply strong star formation disseminated along the ring. In fact, this inner ring must have an older component, since it is also visible in the I band. But the colors of the bluest points in the southeast side of the ring are $B-V\sim0.70$, $V-R\sim0.5$ and $V-I\sim1.05$, suggesting they are H II regions superposed on the older population. Thus the active star formation in the inner ring seems to be restricted to isolated regions, concentrated in the proximity of the leading side of the major axis, and principally in the southeast side. The Hα distribution (Fig. 5) supports this interpretation.

The colors variation along the nuclear ring shows the same amplitude as along the inner ring (0.2 mag in $B-V$), but in this ring all the north side extending to the east is bluer than the south side extending to the west. The mean colors are $B-V=0.86$, $V-R=0.59$, and $V-I=1.25$, that are very similar to the mean colors of the nuclear ring of NGC 3081. One interesting thing with the nuclear ring of IC 4214 is that the two brightest regions that appear in the Hα map have very different colors. The eastern knot (that corresponds nearly to the fifth point in Fig. 12, starting at the point 1 counterclockwise) has colors $B-V=0.80$, $V-R=0.54$, and $V-I=1.14$. These colors, when corrected for color excesses and transformed to the Johnson system to compare with the model by Bica *et al.* (1990), become $(B-V)^{\circ}_{J}=0.66$, $(V-R)^{\circ}_{J}=0.67$, and $(V-I)^{\circ}_{J}=1.27$, that are compatible with H II regions of small mass superimposed to an old stellar

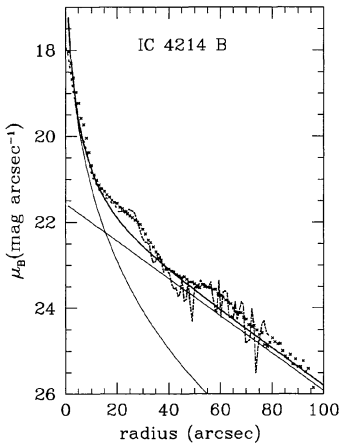

FIG. 13. Decomposition of the B mean surface brightness profile into bulge and disk components. The crosses are the elliptically averaged profile. The thin lines are the bulge and disk functions, and the thick line is the sum of them. For comparison, we also show the folded major axis profile (dotted line). The parameters of each function are listed in Table 6.

population. The western knot (that corresponds nearly to the second point in Fig. 12) has much redder colors: $B-V=0.93$, $V-R=0.64$, and $V-I=1.35$. The differences between the first and forth points is even larger, and the cause probably is the dust lane that departs from the south of the nuclear ring and that gives it the slightly spiral shape. Thus it is possible that the stellar formation is occurring everywhere in the nuclear ring, but is obscured in the south-western part by the dust that is concentrated there.

5.5 Bulge-Disk Decomposition

The images and luminosity profiles of IC 4214 suggest the galaxy has three major components: the bulge, the disk, and the intermediate region where the lens/bar/inner-ring dominates. In an attempt to estimate the contribution of these components to the total luminosity of the galaxy, we determined an elliptically averaged profile to make a bulge-disk decomposition.

The elliptically averaged profile was calculated in the B band only, using the axial ratio and position angle of the external isophotes ($b/a=0.65$, P.A.$=172°$). The profile, shown in Fig. 13, has the appearance of a Type II profile (Freeman 1970), due to the humps produced by the rings. It is well known that these kinds of profiles are not fitted by a sum of a bulge plus an exponential disk, but we assumed that the galaxy has an exponential disk underlying all the complex luminosity distribution, and defined it by the last points in the profile ($r>65''$), plus the points between the inner and outer rings ($40''<r<50''$).

The fit was made using the task *nfit1d* in the STSDAS package, using a sum of an $r^{1/4}$ law (de Vaucouleurs 1948) plus an exponential law (Freeman 1970). We neglected the points corresponding to the seeing ($r<2.3''$), to the intermediate region ($15'' < r < 40''$), and also to the outer ring region ($50'' < r < 65''$). Since the elliptically averaged profile stretches the radius corresponding to each surface brightness in the bulge region (due to the smaller ellipticity of the bulge isophotes compared to the disk isophotes), we used the profile averaged in ellipses (that is similar to the major axis profile in the bulge region, but smoother) to determine the parameters of the bulge. The scale length of the disc was determined in the disk region of the elliptically averaged profile (up to $r=95''$), assuming no bulge contribution, and then was kept fixed.

TABLE 6. Derived parameters for the bulge and disk components of IC 4214.

	Bulge[a]	Disk[a]
Fit region (arcsec)	2.5–14.5	40–80
Fit parameters	$\mu_e=20.49$	$\mu_0=21.57$
	$r_e=7.2$ arcsec	$r_0=25.0$ arcsec
Total luminosity	$1.42\times10^{10}L_\odot$	$1.15\times10^{10}L_\odot$
Fractional luminosity ($L/L_{\rm total}$)	0.44	0.36
Absolute magnitude	−19.90	−19.67

[a]All parameters refer to the B filter.

The best fit (Fig. 13) obeys the equations:

$$\mu_B(\text{bulge})=20.49+8.325[(r/7.2)^{1/4}-1],$$

$$\mu_B(\text{disk})=21.57+1.0857(r/25),$$

where surface brightness is given in mag/arcsec^2 and the radius in arcsec.

As pointed out by Byun & Freeman (1995), the decomposition based on elliptically averaged profiles is subject to strong systematic errors associated with the derivation of the profile, that is not unique. These errors might be even larger in the present case, where we had to neglect so many points of the profile. So we are not claiming that these parameters are the true parameters of the bulge and disk of the galaxy, but that they represent reasonably well the basic luminosity of the galaxy, and are compatible with usual parameters of bulge and disk. So we believe they can give rough idea of the contribution of these two components to the total light of the galaxy.

Correcting the effective surface brightness of the bulge only for galactic extinction A_B (Simien & de Vaucouleurs 1986—SdV86), and the extrapolated central surface brightness of the disk by galactic extinction and inclination effects [SdV86; Kent 1985; Boroson (1981)], and adopting the RC3 value for A_B (see Table 1) and the axial ratio of disk derived from the ellipse fitting (see Table 5), the corrected parameters are $\mu_e^c(\text{bulge})=20.23$, and $\mu_0^c(\text{disk})=21.77$. The later is in good agreement with the mean value of 21.65 found by Freeman (1970).

The total luminosity of each component, calculated according to de Vaucouleurs (1974), for the bulge, and Freeman (1970), for the disk, gives a bulge to disk ratio of $B/D=1.23$; the corresponding total magnitudes, $M_B(\text{bulge})=-19.90$, and $M_B(\text{disk})=-19.67$, agree with the mean values of these parameters measured by SdV86, within the errors quoted by them. The two components together contribute 80% of the total luminosity of the galaxy, $M_B(\text{total})=-20.81$. The remaining 20% must be accounted by the components that dominate in the intermediate region.

Table 6 collects the derived photometric parameters for the bulge and disk components.

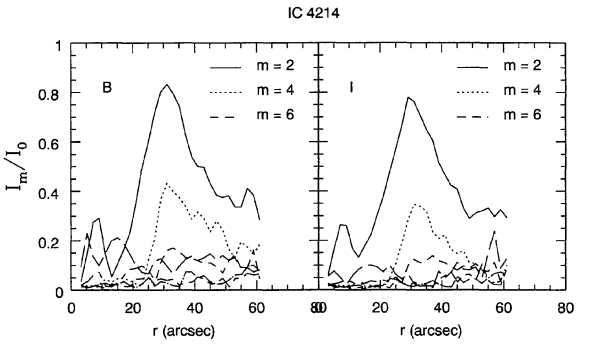

FIG. 14. Relative Fourier intensity amplitudes for IC 4214 in the *B* and *I* bands. The terms $m=1$, 2, 3, 4, 5, 6 are plotted, but no odd terms are significant.

5.6 Fourier Analysis

In order to obtain more information on the luminosity distribution of IC 4214, we made a Fourier decomposition following Odewahn (1991), averaging the light distribution within elliptical annuli with the same position angle an axial ratio as the external isophotes, and modeling it by a Fourier series with a sinusoidal basis. The Fourier amplitudes are illustrated in Fig. 14, for the *B* and *I* bands. Only the even terms $m=2$ and $m=4$ are important, possibly because the occasional asymmetries in the galaxy are masked due to the inclination. The amplitude profiles are very similar to those of NGC 3081 (Buta 1991a), presenting two separated peaks. The first and smaller one occurs at $r=15''$, corresponding to the elongated bulge region, and reaches $I_2/I_0 \sim 0.25$ in *B* and in *I*. The second and stronger peak occurs around $r=30''$, in the border of the inner pseudo-ring/lens, where the relative amplitude I_2/I_0 reaches 0.83 in *B* and 0.78 in I. Amplitudes this high are more typical of strong barred galaxies like NGC 4314 and NGC 7479 (Elmegreen & Elmegreen 1985), NGC 1433 (Buta 86), and NGC 5757 (Saraiva Schroeder *et al.* 1994), and indicate that IC 4214 has a strong oval distortion despite the bar being weak. Using Eq. (6) in Buta (1986b) to derive the fractional contribution of the non-axisymmetric component with respect to the accumulated luminosity of the galaxy, then the oval, defined only by the components $m=2$ and $m=4$, contributes 22% of the *B* luminosity within $r=80''$, and 23% of the *I* luminosity within the same radius. These values agree reasonably well with those expected from the bulge-disk decomposition.

5.7 Bar-like Features in IC 4214

IC 4214, despite not having a strong bar, apparently has four different bar-like features: the nuclear elongation (Fig. 8), the *I* bar (Fig. 7), the ring/lens region (Fig. 3), and the pointed oval region (Fig. 2), which, depending on the contrast level of the image, may looks like a big bar.

The small nuclear bar, if real, hardly could be confused with a main bar. Nevertheless, it may be difficult to decide, based only on the appearance of the galaxy, what of the other three features is the bar in IC 4214.

In an attempt to characterize these structures, we calculated the metric parameters defined by Martin (1995) for the three of them, and compared them to general properties of bars. The parameters are listed in Table 7, where a and b are the major and minor semi axes of the bar structure, ϕ_a is the angle between the disk major axis and the bar major axis, L_B is the bar length relative to the corrected diameter of the galaxy at 25 mag $^{-2}$, D_0, as given in the RC3, and $2b/D_0$ is the defined bulge size. The corrections for inclinations were made as in that paper.

Since the galaxy has a high inclination (51^o), the corrected values b/a(i) and L_B(i) differ significantly from the observed values, and should be taken with caution. Furthermore, the statistics of Martin are very poor for galaxy types earlier than *Sb*. With these restrictions in mind, we made a comparison of the parameters with Figs. 5 (L_B(i) vs T) and 9 (L_B(i) vs $2b/D_0$) of Martin (1995). We found that the relative length of the bar/inner ring regions is typical of Sa-Sab, and fits well in the linear relation between bar length and bulge diameter. The same happens in the case of the primary lens. In the case of the pointed oval, its bar length seems to be too large, but cannot be considered abnormal considering the dispersion of the sample in the figure. It also fits the relation bar length versus bulge diameter, if we extrapolate this relation for larger values.

Therefore, according to these parameters, these three structures could be considered bars, or weak bars. This shows how large is the variety of sizes that has been attributed to bars, and stresses the necessity of using non-subjective parameters for bar identification. In this paper, we took into account that observations have shown that whenever a galaxy has a bar and a inner ring, the bar never overfills the inner ring (Buta, private communication), so the galactic bar of IC 4214 should be the *I* bar. Could this small, weak bar have generated resonances strong enough to produce the three rings, or did IC 4214 once have a stronger bar?

The increasing number of observed galaxies with rings and no visible bar does suggest that even very weak oval distortions can manage to form rings (e.g., Buta *et al.* 1995). But, as it seems to have occurred in other similar cases cited in the introduction of this work, it is possible that the rings formed in the past, when the bar was stronger. Subsequently it evolved to the lens that is observed around the inner ring,

TABLE 7. Metric parameters of the oval regions in IC 4214.

Feature	(″)	b/a	ϕ_a(°)	b/a(i)	L_B	L_B(i)	$2b/D_0$
bar/inner ring	26	0.46	20	0.65	0.41	0.45	0.19
primary lens	35	0.50	20	0.70	0.51	0.55	0.25
pointed oval	50	0.50	20	0.70	0.71	0.77	0.35

TABLE 8. Hα and V relative flux within the nuclear region.

A(″)[a]	F_H(nucl)/F_H(A)	F_V(nucl)/F_V(A)
160	0.21	0.22
80	0.30	0.28
5	2.90	2.10

[a]Diameter of the region of the galaxy, centered on the nucleus, where the flux was measured.

by the process of bar-to-lens evolution suggested by Kormendy (1979).

5.8 The Nuclear Emission

In order to estimate the importance of the emission in the nuclear region of IC 4214, we measured the flux of the nuclear region (up to the outer limits of the nuclear ring) relative to different regions of the galaxy. The measurements are collected in Table 8. For a comparison of the emission flux with the continuum flux, we made the same measurements also in the V passband. We found that the Hα flux within the nuclear region relative to the total Hα flux from the galaxy is 0.21; Pogge (1989) measured this fraction for 12 galaxies where the nuclear emission was concentrated in the nuclear rings, and found $F_{\rm nuc}/F_{\rm total}$ varying from 0.01 to 0.94, with 6 of the galaxies having this ratio between 0.1 and 0.2. Thus we conclude that the Hα flux of the nuclear region of IC 4214 is fairly normal. The comparison of the flux ratios in Hα with the flux ratios in V shows that the emission follows the same pattern of the stellar flux, except inside the nuclear region, where the importance of the nuclear ring relative to the nucleus is greater in Hα than in V.

5.9 Comparison with NGC 3081

The structure of IC 4214 is similar to that of the galaxy NGC 3081 in many aspects. Both contain a weak bar, three rings, dust lanes, and some pieces of evidence of the existence of a nuclear bar. The main differences between them are the earlier type of NGC 3081, its smaller inclination, and the fact that NGC 3081 is a Seyfert, and IC 4214 is at best a LINER.

The rings in both galaxies have similar sizes, with sizes-ratios consistent with they being associated with the principal resonances.

The inner ring is very elongated in the two galaxies, with axis ratio similar to the inner ring of the strong barred galaxy NGC 1433. Buta (1990a) interpreted the fact that both NGC 3081 and NGC 1433 have inner rings with similar ellipticity as an indication that the ellipticity of the inner ring is not correlated with the strength of the bar. In fact, the same author found in the CSRG (1995) that the intrinsic axial ratio of inner rings of SAB galaxies is in average *more elliptical* than in SB galaxies.

Both galaxies have azimuthal color variation along the inner ring, but the locations of the bluest and reddest regions respect to the major axis of the ring are different: in NGC 3081 the H II regions are concentrated in arcs at the major axis, while in IC 4214 they are more concentrated in the leading side of the major axis. Also, the mean color of the inner ring of IC 4214 is not as blue as that of NGC 3081, despite the fact that the whole gas content of IC 4214 must be higher. In both galaxies the inner ring has an old ring and/or a lens associated to it.

The nuclear ring of both galaxies have similar mean colors and are very prominent in the $B-I$ maps, but the nuclear ring of IC 4214 is also prominent in the Hα map and that of NGC 3081 is not [in NGC 3081 the nuclear Hα emission fills the entire nuclear zone, as can be seen in the map by Wosniak *et al.* (1995), while in IC 4214 the distribution is more like that of NGC 4314 (Pogge 1989)].

The Fourier amplitude profiles of both galaxies are very similar, in shape and in amplitude height. For both, the amplitudes produced by the bar itself is low, but the amplitude produced by the inner ring region is comparable to that of strong barred galaxies. It seems that both galaxies are going through a similar evolutionary process.

6. SUMMARY OF RESULTS

We report *BVRI* and Hα CCD photometry for IC 4214, a weakly barred galaxy with the three ring types possible in a galaxy: a nuclear ring, an inner ring and a faint outer ring. Its total B magnitude obtained from the elliptical averaged profile is $B_T=12.27$. For a distance of 31 Mpc it corresponds to an absolute magnitude corrected by Galactic and internal absorption of $M^{\circ}_T=-20.81$. The $B-V$ corrected color is 0.74, consistent with its morphological type. The galaxy has many morphological and photometric properties in common with other barred and weakly barred galaxies, mainly with NGC 3081.

The analysis of the mean profile shows that the galaxy has three main structural components: the nuclear bulge, the disk, and an intermediate region that is a mixture of bar, inner pseudo-ring and lens. The bar is small and clearly visible only in the I band, suggesting it is populated by old stars.

The bulge presents twisted isophotes with distorted oval-rectangular shapes that suggest it is triaxial or/and contains a nuclear bar.

The inner ring is the most elongated feature in the galaxy, with an intrinsic ellipticity higher than the average ellipticity of inner rings in SB galaxies. It is blue compared with its surroundings, and contains sites of star formation concentrated in the leading sides of its major axis, although it must contains also an older stellar component underlying it.

The nuclear ring is a round blue feature, very prominent in Hα, that seems to be composed of H II regions mixed with dust.

A Fourier analysis with a sinusoidal basis showed that the $m=2$ and $m=4$ components have a maximum at the surroundings of the inner ring, but are significantly important out to the ends of the spiral arms region (pointed oval). The fractional contribution of these components with respect to the accumulated I luminosity within the radius of 80″ is 23%.

The fact that the galaxy has a small and possibly old bar, added to the fact that the inner ring is embedded in a lens that comprises the zone with dominant non-axisymmetric

term in the galaxy, suggest that IC 4214 is another example of a galaxy that is going on though a process of bar dissolution. The lens would be the result of this process.

I wish to address a special note of appreciation to the late Gerard de Vaucouleurs, for his wise suggestions at the beginning of this work. I would like to thank Steve Odewahn, for kindly giving me the Numerical Mapping Technique code and help-ing me with its use, Ron Buta, for a useful discussion, Kepler Oliveira, Fritz Benedict, and Inger Jørgensen for their careful reading and helpful comments on the first version of this manuscript, and Horacio Dottori and Basilio Santiago for a useful suggestion. I thank very much the anonymous referee for several comments and suggestions that allowed me to improve this work. I acknowledge the Brazilian institution CNPq for a fellowship.

REFERENCES

Athanassoula, E. 1992, MNRAS, 259, 345
Athanassoula, E. 1996, in Evolution of Bars in Isolated and in Interacting Disk Galaxies, Barred Galaxies, IAU Colloquium 157, edited by R. Buta, D. A. Crocker, and B. G. Elmegreen ASP Conf. Ser. 91 (ASP, San Francisco), p. 309
Athanassoula, E., Bosma, E., Crézé, M., & Schwarz, M. P. 1982, A&A, 107, 101
Baumgart, C. W., & Peterson, C. J. 1986, PASP, 98, 56
Benedict, G. F., Higdon, J. L., Tollestrup, E. V., Hahn, J., & Harvey, P. M. 1992, AJ, 103, 757
Bica, E., Alloin, D., & Schmidt, A. 1990, MNRAS, 242, 241
Boroson, T. 1981, ApJS, 46, 177
Bottinelli, L., Gouguenheim, L., Paturel, G., & de Vaucouleurs, G. 1983, A&A, 418, 4
Burstein, D. 1979, ApJ, 234, 435
Buta, R. 1995, ApJS, 96, 39 (CSRG)
Buta, R., van Driel, W., Braine, J., Combes, F., Wakamatsu, K., Sofue, Y., & Tomita, A. 1995, ApJ, 450, 593
Buta, R., & Crocker, D. A. 1991, AJ, 102, 1715
Buta, R., & Crocker, D. A. 1992, AJ, 103, 1804
Buta, R., & Crocker, D. A. 1993, AJ, 105, 1344
Buta, R. 1990a, ApJ, 351, 62
Buta, R. 1990b, ApJ, 354, 428
Buta, R. 1990c, ApJ, 356, 87
Buta, R. 1990d, ApJ, 370, 130
Buta, R. 1986a, ApJS, 61, 609
Buta, R. 1986b, ApJS, 61, 630
Byun, Y. I., & Freeman, K. C. 1995, ApJ, 448,
Combes, F. 1996, in Ring and Lens Formation, Barred Galaxies, IAU Colloquium 157, edited by R. Buta, D. A. Crocker, and B. G. Elmegreen, ASP Conf. Ser. 91 (ASP, San Francisco), p. 286
Crocker, D. A., Baugus, P. D., & Buta, R. 1996, H II Regions in Resonance-Ring Spiral Galaxies, Barred Galaxies, IAU Colloquium 157, edited by R. Buta, D. A. Crocker, and B. G. Elmegreen, ASP Conf. Ser. 91 (ASP, San Francisco), p. 80
de Vaucouleurs, G. 1948, Ann. d'Ap, 11, 247
de Vaucouleurs, G. 1974, ApJS, 29, 193
de Vaucouleurs, G. 1977, in The evolution of Galaxies and Stellar Populations, edited by B. Tinsley and R. Larson (Yale University Observatory, New Haven), p. 43
de Vaucouleurs, G., de Vaucouleurs, A., Corwin, Buta, R., Paturel, G., & Fouqué, P. 1991, The Third Reference Catalogue of Bright Galaxies (Springer, New York) (RC3)
Elmegreen, B. C., & Elmegreen, D. M. 1985, ApJ, 288, 438
Freeman, K. C. 1970, ApJ, 160, 811
Forbes, D. A., & DePoy, D. L. 1992, A&A, 259, 97
Graham, 1982, PASP, 94, 244
Hackwell, J., & Schweizer, F. 1983, ApJ, 265, 643
Han, M. 1992, ApJS, 81, 35
Jones, W., Obitts, D., Gallet, R., & de Vaucouleurs, G. 1967, Astronomical Surface Photometry by Numerical Mapping Techniques, Publications of the Department of Astronomy or the University of Texas at Austin Series II, Vol. 1, No. 8
Kent, 1985, ApJS, 59, 115
Kormendy, J. 1982, in Observations of Galaxy Structure and Dynamics, Morphology and Dynamics of Galaxies, edited by L. Martinet and M. Major (Geneva Observatory, Sauverny), p. 113
Maia, M. A. G., da Costa, L. N., Willmer, G., Pellegrini, P. S., & Rité, C. 1987, AJ, 93, 546
Martin, P. 1995, AJ, 109, 2428
Odewahn, S. C. 1991, AJ, 101, 829
Ohta, K., Hamabe, M., & Wakamatsu, K.-I. 1990, ApJ, 357, 71
Pogge, R. 1989, ApJ, 71, 433
Palouŝ, J., & Jungwiert, B. 1996, in Multiple Gas Rings in SA Galaxies, Barred Galaxies, IAU Colloquium 157, edited by R. Buta, D. A. Crocker, and B. G. Elmegreen, ASP Conf. Ser. 91 (ASP, San Francisco), p. 369
Rush, B., Malkan, M., & Spinoglio, L. 1993, ApJS, 89, 1
Saraiva Schröder, M. F., Pastoriza, M. G., & Kepler, S. O. 1994, A&AS, 104, 487
Schröder, M. F. S., Pastoriza, M. G., & Kepler, S. O. 1990, PASP, 103, 383
Shaw, M., Axon, D., Probst, R., & Gatley, I. 1995, MNRAS, 274, 369
Simien, F., & de Vaucouleurs, G. 1986, ApJ, 302, 564
Tammann, G. A., & Sandage, A. 1985, ApJ, 294, 81
Thronson, H. A., Hereld, M., Majewski, S., Johnson, P., Spillar, E., Woodward, C. E., Harper, D. A., & Rauscher, B. J. 1989, ApJ, 343, 158
Wosniak, H., Friedli, D., Martinet, L., Martin, P., & Bratschi, P. 1995, A&AS, 111, 115